Chapter 3

VISCOELASTIC PHASE PATTERNING IN ARTIFICIAL PROTEIN HYDROGELS

3.1 Abstract

Viscoelastic forces can affect the dynamics of pattern formation during phase separation in polymeric materials. We programmed an artificial protein hydrogel to undergo viscoelastic phase separation above a critical temperature set point. Highly dynamic phase patterns that coarsened under the influence of a mechanical stress balance spontaneously emerged in these gels. Mild oxidative crosslinking promoted by photobleaching initialized the phase change locally, enabling patterning of non-equilibrium phase shapes into phase separating gels. Subsequent pattern evolution illustrated that a delicate balance of surface tension and viscoelastic stress controls pattern formation in viscoelastic materials.

3.2 Introduction

Phase separation can induce spontaneous pattern formation in polymeric materials (*1*). This provides a simple way to control material microstructure, enabling access to diverse and useful material properties (*2*-*4*). Simple solids and liquids develop either a bicontinuous or a droplet pattern in transition to a binary equilibrium state (*5*). Unique web- and sponge-like patterns can emerge in viscoelastic materials, which have dynamic properties intermediate between fluids and solids (*5*-*7*). Whereas pattern growth in simple mixtures is often scale invariant or “self-similar” (*8*), stress relaxation in viscoelastic materials can break the self-similarity or scale invariance of developing patterns (*9, 10*).

3.3 Results and Discussion

3.3.1 Sequence programmable phase separation in an artificial protein hydrogel

Thus far, viscoelastic effects on phase separation have been recognized in several isolated contexts (*6, 9, 11-14*), but remain difficult to predict and control. We hypothesized that artificial proteins could be programmed to routinely undergo viscoelastic phase separation by encoding them with two key features: *i*) the ability to self-assemble into a reversible network that stores and dissipates mechanical stress and *ii*) a phase transition temperature set point. Accordingly, we cloned and expressed a large (32 kDa), artificial protein polymer designated "PEP" that aimed to satisfy these criteria (**Figure 3.1A** and **Supplementary Table 3.1**). PEP comprises a flexible, water-soluble "E" midblock encoding 30 repeats of the elastin-like pentapeptide sequence $(VPGXG)_n$, where X is either V or E. This domain is flanked by two coiled-coil forming "P" endblocks (*15*) that promote reversible self-assembly of the protein monomer into a viscoelastic hydrogel (**Figure 3.1A** and **Supplementary Figure 3.1**) (*16-18*). We intended for the midblock to confer tunable phase behavior to these networks, owing to the thermally-induced phase transition above a lower critical solution temperature (LCST) that is a well-known property of elastins (*19-21*).

Based on the sequence of E, we predicted that PEP networks would display a simple, LCST-type phase transition at 70 °C (*21*). Surprisingly, cloud-point measurements were indicative of phase separation at much lower temperatures (*22*): at 38 °C, 5% (*w*/*v*) PEP gels separated into an aqueous phase (A) and a protein-rich coacervate phase (C) (**Figure**

3.1B). Moreover, the gels also exhibited reentrant behavior: continued heating above 64 °C completely restored protein miscibility, and a second cloud-point (UCST) became evident upon subsequent cooling. Similar measurements at other concentrations revealed an immiscibility loop in the *T*-φ phase diagram and an apparent critical composition near 5% (ϕ_c, **Figure 3.1C**). Phase diagrams of this class are rare (*23-27*), but are predicted from Flory theory when the polymer-solvent interaction parameter χ exceeds a critical value χ_c over a finite temperature range (*26*).

In an effort to understand this unexpected phase behavior, we performed cloud-point measurements on two additional engineered proteins (**Supplementary Table 3.1**). Concentrated solutions of a free, uncrosslinked "E" protein underwent phase separation near 85 °C, closer to the LCST predicted from sequence (**Supplementary Figure 3.2**). Using site-directed mutagenesis, we installed a single cysteine within this protein to promote disulfide crosslinking under oxidizing conditions. Dimerized solutions of this "E_C" protein displayed a depressed LCST at 63 °C (**Supplementary Figure 3.2**). These results imply that covalent and non-covalent interchain associations can significantly reduce the native transition temperature of elastins (*22, 23*). We attribute the reentrant behavior of PEP gels to gradual thermal unfolding of the P endblocks between 25 °C and 65 °C (*28*). Unfolding was evident from the mechanical softening of gels during heating (**Supplementary Figure 3.1**).

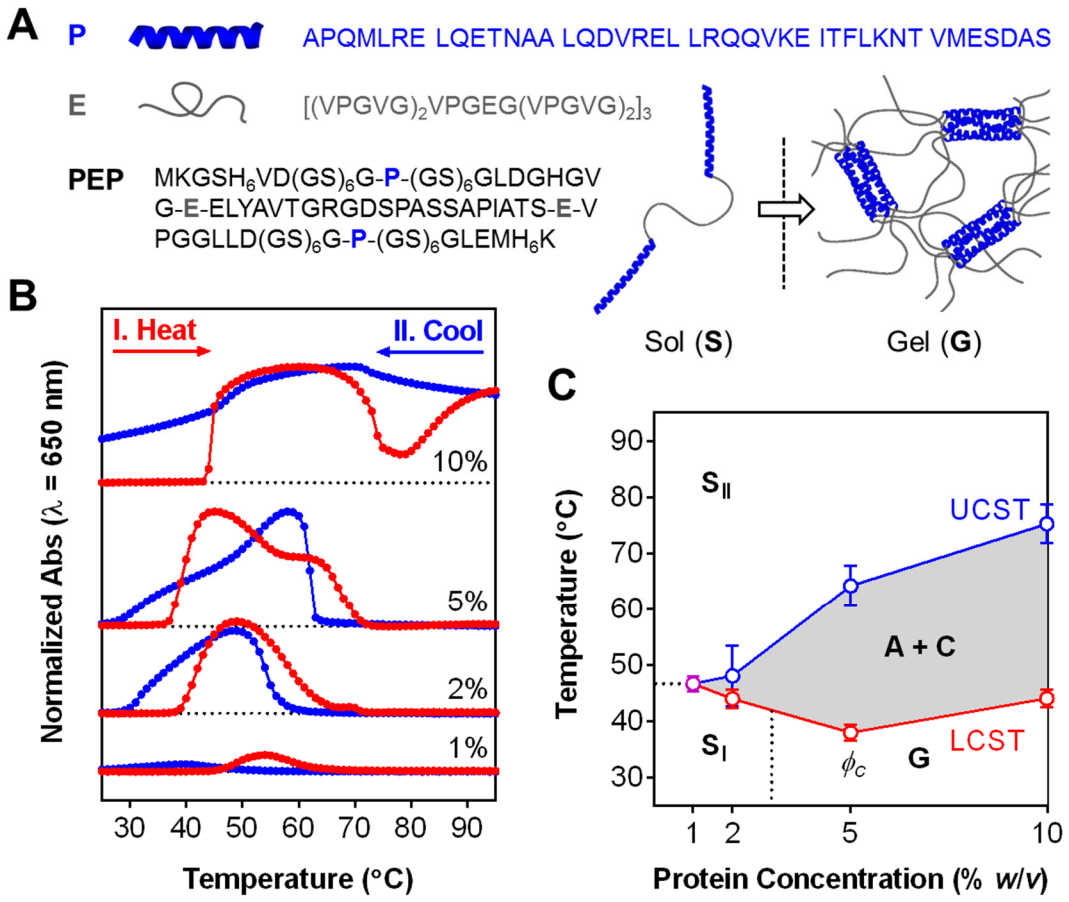

Figure 3.1. Sequence programmable phase separation in an artificial protein hydrogel. (**A**) Sequence of PEP. The protein comprises two coiled-coil forming "P" endblocks which flank a water soluble elastin-like "E" midblock. When swollen in aqueous buffer, the oligomerization of the endblocks drives reversible self-assembly into a viscoelastic gel. (**B**) Cloud-point measurements on PEP gels (pH 6.5) reveal phase separation and reentrant behavior (UCST > LCST). The gels were first heated then cooled over the range 25 °C to 95 °C at a rate of 3 °C min^{-1}. Gel turbidity was monitored at 650 nm. (**C**) The *T*-*φ* phase diagram of PEP contains an immiscibility loop: S_I, sol phase; G, reversible gel; A + C, aqueous phase (protein-poor) and coacervate phase (protein-rich); S_{II}, reentrant sol phase. Points represent mean ± SD (n = 4).

3.3.2 Influence of viscoelastic stress on domain coarsening in PEP hydrogels

Next, we labeled PEP networks with a fluorescent, associative phase probe (PEcP-*fm*, **Supplementary Figure 3.3**) in order to visualize pattern evolution during phase separation above the LCST. Following rapid heating to 50 °C, phase boundaries formed and the gel began to shrink. The developing coacervate (protein-rich) phase initially resisted this collapse by generating a transient, elastic restoring force. This caused the dramatic emergence of a highly interconnected, sponge-like structure that condensed as the stress relaxed (**Figure 3.2A**). Remarkably, coarsening by aqueous droplet coalescence internal to the coacervate completely reconfigured this early stage pattern over a period of several hours (**Figure 3.2B**). The resulting late stage pattern appeared to lack any characteristic length scale, as new aqueous droplets could still be seen nucleating within the coacervate.

This unusual type of pattern evolution is a hallmark of phase separation under the influence of viscoelastic stress (*29*). Tanaka has proposed that such web- and sponge-like patterns arise whenever the phase separation rate is faster than the internal stress relaxation rate of one of the phases (*6, 30*). Under these circumstances, early domain shape evolves to satisfy a mechanical force balance. Subsequent viscoelastic stress relaxation generates elastic instabilities that promote domain breakage. Simultaneously, regular coarsening modes (e.g., droplet ripening) erode the domains into circular architectures in order to minimize interfacial tension. The presence of multiple coarsening modes, each dominating at different times, breaks the self-similarity of the phase decomposition, producing irregular features with divergent length scales (*9, 10, 30*). Our results are in qualitative agreement with this picture.

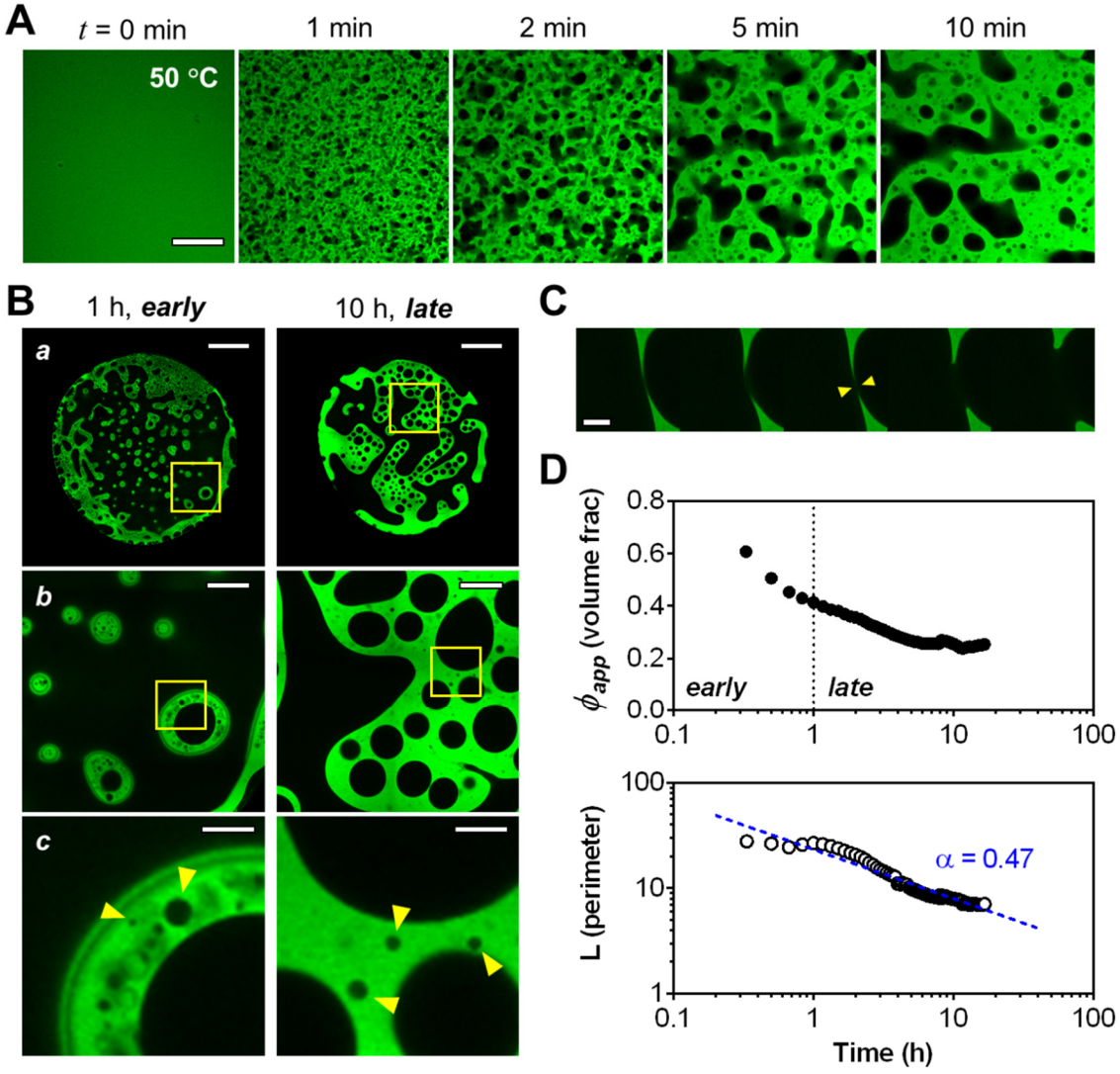

Figure 3.2. Viscoelastic phase separation in PEP hydrogels. (**A**) Rapid heating of 10% PEP gels to 50 °C promotes the emergence of a transient sponge-like phase within the first 10 min. Scale bar = 100 μm. (**B**) Overview images of early (1 h) and late (10 h) stage coarsening at several magnification levels reveal the absence of a characteristic length scale and the presence of multiple coarsening modes. Scale bars: (*a*) 1 mm, (*b*) 200 μm, (*c*) 50 μm. (**C**) Viscoelastic "breakage" events relaxed local domain configuration during the late stage (shown are five frames taken over 10 min, after 8 h of heating). Scale bar = 50 μm. (**D**) Quantitative analysis of pattern evolution. (*Top*) The volume fraction of the protein-rich coacervate phase decreased well into the late stage, violating a

prerequisite for self-similar domain growth. (*Bottom*) The interface line density (normalized total perimeter) obeyed an approximate power law of the form $L \sim t^{-\alpha}$ ($\alpha = 0.4 \pm 0.1$, $n = 4$).

Several additional features of late stage pattern evolution support the persistence of a viscoelastic coarsening mode. We routinely observed viscoelastic breakage events lasting several hours, in which slender coacervate tendrils "snapped" back to relax internal stress (**Figure 3.2C**). The apparent volume fraction of the coacervate phase obtained by image thresholding analysis decreased well into the late stage, implying a slowly changing phase composition (**Figure 3.2D**). This violates a prerequisite for scale invariant domain growth (*8, 9*), and suggests suppression of interphase diffusion by an elastic energy barrier. Finally, the total interfacial perimeter decayed following an approximate power law ($\alpha = 0.4 \pm 0.1$, **Figure 3.2D**). This is consistent with late stage growth dominated by either droplet ripening or fusion ($\alpha = ⅓$) (*30, 31*). Both growth mechanisms were clearly discernible by time-lapse microscopy, with aqueous droplet fusion visibly frustrated by the viscoelastic nature of the coacervate.

3.3.3 Photobleaching perturbs local phase domain morphology

We envisioned that our fluorescence-based phase visualization strategy might also lend itself to quantifying diffusion during phase separation via fluorescence recovery after photobleaching (FRAP). This technique has been widely used to characterize macromolecular transport within hydrogels (*32, 33*), and we recently applied it to study the mechanism of chain migration in PEP networks below the LCST (*18*). Consistent with our previous study, gels labeled with the associative phase probe PE$_C$P-*fm* (**Supplementary**

Figure 3.3) showed steady fluorescence recovery at 25 °C, implying diffusive chain migration through the network (**Figure 3.3A**).

In contrast to this simple diffusive behavior, the fluorescence recovery behavior of gels photobleached near the phase boundary was highly anomalous. During phase separation onset at 40 °C, photobleaching clearly perturbed the local domain structure, tending to induce the formation of thin coacervate spines around the bleach spot (**Figure 3.3A**). The rate of fluorescence recovery during the early stage appeared accelerated relative to the late stage (**Figure 3.3B**). Moreover, both the early and late stage recovery profiles were poorly fit by a standard FRAP model that attributes fluorescence recovery to simple diffusion (**Supplementary Figure 3.4**) (*34*).

To explore the origin of the anomalous recovery behavior, we performed photobleaching experiments with two, spectrally independent phase probes. Photobleaching of a green probe (PEcP-*fm*, 490Ex/525Em) triggered diffusion of an unbleached red probe (PEcP-*trm*, 596Ex/615Em) into the bleach spot (**Supplementary Figure 3.3A**). Fluorescein and rhodamine-based dyes are known to readily generate singlet oxygen (*35, 36*), a highly reactive oxygen species that that rapidly crosslinks proteins (*37-39*). We observed that prolonged irradiation of labeled gels promoted oxidative crosslinking of PEP chains *in situ* (**Supplementary Figure 3.3B**). Crosslinking and bleach spot enrichment were completely suppressed by sodium azide, a strong singlet oxygen quencher. Taken together, these results implicate mild oxidative crosslinking by photobleaching as the origin of the anomalous recovery behavior. Our cloud-point measurements (**Supplementary Figure 3.2**

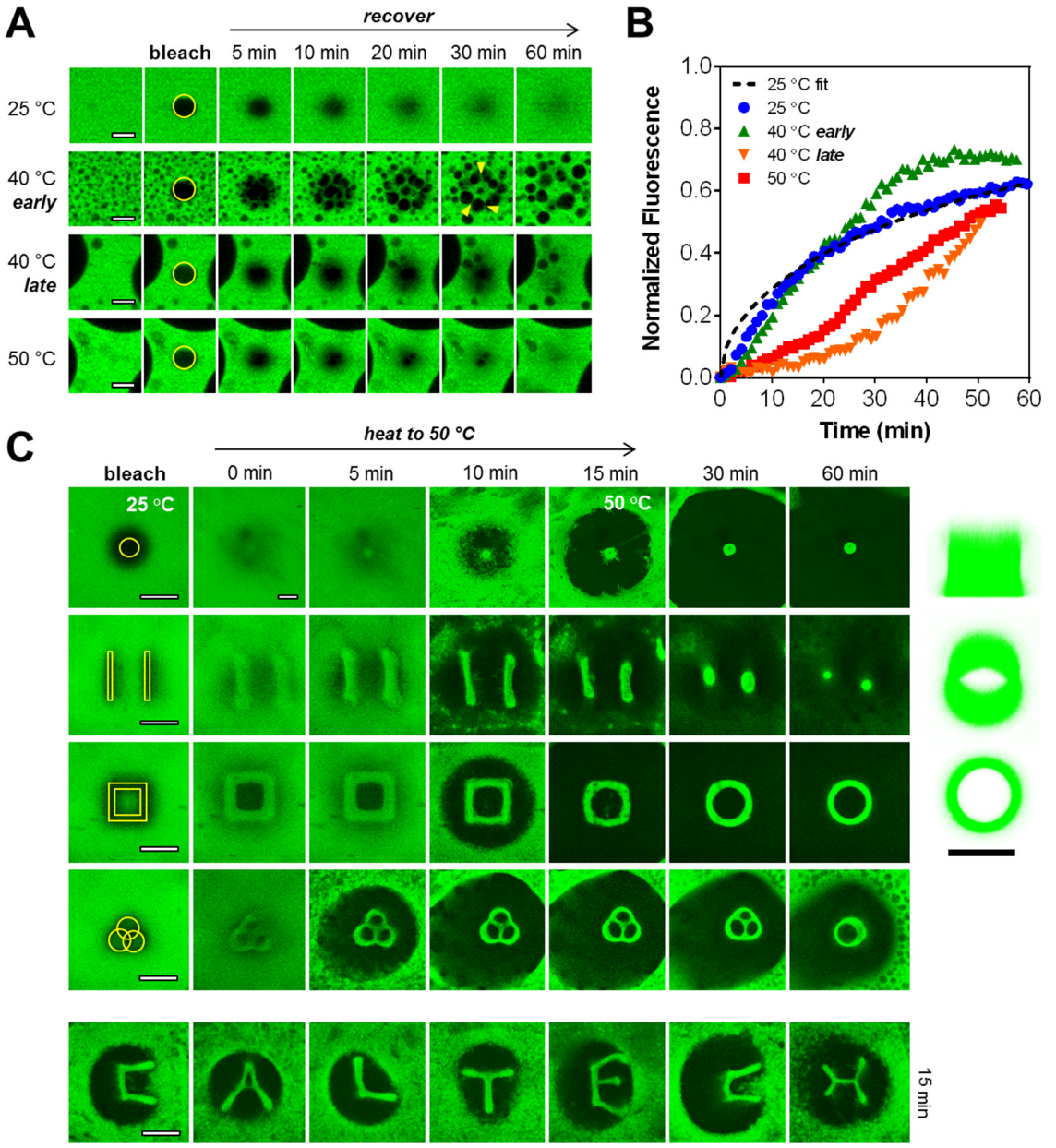

Figure 3.3. Photobleaching enables patterning of dynamic phase shapes during phase separation onset. (**A**) Fluorescence recovery after photobleaching (FRAP) was monitored in 10% gels at temperatures below (25 °C) and above (≥ 40 °C) the phase transition temperature (LCST). Photobleaching perturbed local domain structure in gels recently heated to this temperature (40 °C *early,* 30 min). Scale bars = 20 μm. (**B**) Anomalous fluorescence recovery behavior above 40 °C. (**C**) Heating of 5% gels after photobleaching matured the photobleached regions into dynamic

coacervate domains. The patterned domains evolved under the control of interfacial tension and a quickly relaxing mechanical stress, gradually producing (equilibrium) cylindrical and droplet phase architectures. Scale bars = 100 μm.

---

and **Figure 3.1B**) argue that crosslinked chains can have a depressed LCST (*19*). Crosslinking by photobleaching is apparently sufficient to trigger a local phase change below the global phase transition temperature, with subsequent chain enrichment in the bleach spot in order to equalize the chemical potential at the bleach spot boundary.

Photobleaching prior to the onset of phase separation had a pronounced effect on the local phase domain morphology (**Figure 3.3C**). After a brief recovery period, heating to 50 °C induced early maturation of the bleach spots into patterned coacervate domains. Rapid contraction of the global coacervate above the network LCST then caused viscoelastic tearing around the bleach spot, which isolated the patterns in a wide depletion zone. During this period, the patterns behaved as soft elastic bodies and appeared stretched by a radially symmetric stress that pulled them towards the receding coacervate boundary. This tended to create non-equilibrium coacervate structures exhibiting mild distension along concentric lines (e.g., the equiangular vertices of a photobleached “H” character). Ongoing stress relaxation and volume shrinking subsequently collapsed the patterns into symmetrical droplet and cylindrical structures that were gradually absorbed by the global coacervate.

3.4 Conclusion

We programmed an artificial protein hydrogel with viscoelastic phase behavior. The ability of the network to both store and dissipate mechanical stress induces unusual sponge-like

phase patterns, and causes a breakdown in the scale invariance of the phase decomposition. Pattern evolution is governed by a delicate balance of surface tension and viscoelastic stress, and mild oxidative crosslinking can perturb this balance in a striking manner. In light of the ability to tune the stress relaxation dynamics of artificial protein networks using protein engineering (*40*), it will be interesting to explore the extent to which such patterning can be further controlled by changes to protein sequence.

3.5 Acknowledgements

The assistance of Andres Collazo of the Beckman Imaging Center at the California Institute of Technology is gratefully acknowledged. We also thank Cole DeForest, John Bagert, and Kai Yuet for helpful discussions during the preparation of this chapter. Support from the NSF is also very gratefully acknowledged.

3.6 Supporting Information

3.6.1 Materials and Methods

Protein expression and purification. Plasmids encoding the artificial proteins were transformed into BL21 or BL21 (DE3) chemically competent *E. coli*. After overnight culture, cells were inoculated (inoculation ratios of 1:50 – 1:100) into 1 L flasks containing Terrific Broth (TB) supplemented with 100 – 200 mg ml^{-1} ampicillin. Cells were grown to an OD_{600} of 0.8 – 1.0 and then induced with 1 mM final concentration of isopropyl β-D-1 thiogalactopyranoside (IPTG). After 4-5 h, bacterial cultures were harvested by centrifugation for 5-10 min at 10,000*g*, followed by lysis with 8 M urea. Cell lysates were freeze-thawed at least once before being subject to high-power tip sonication for homogenization (50 mL of lysate from a 1 L culture was typically treated with 30 – 50 W for 10 min in 0.5 s pulses). Homogenized lysate was clarified by high-speed centrifugation (>30,000*g* for 1 h) and then subject to standard His-tag purification over Ni-NTA agarose beads (Qiagen) under denaturing conditions (8 M urea).

Protein dialysis and refolding. Denatured, His-purified protein (50 – 100 mL in 8M urea and phosphate buffer) was dialyzed against 4 L of distilled water at 4 °C. The water was changed repeatedly (5 – 6X) over the course of several days. Typically, protein precipitation within the dialysate was used as the dialysis endpoint, after which point the aqueous suspensions were lyophilized. This procedure routinely gave gels that displayed cloud points near 40 °C (cf. **Figure 3.1C**). However, subtle changes to the refolding procedure (e.g. changes in dialysis temperature, buffer identity or exchange rate) could significantly shift

this transition temperature. A slow buffer exchange rate starting in urea and phosphate buffer could depress the LCST to below 25 °C. Fast dialysis starting in urea and Tris buffer made the temperature transition undetectable by turbidimetry. We infer that our observed LCST is not a simple function of elastin sequence E, but depends strongly on the folded state of the P endblocks, and on their interactions with E.

Hydrogel preparation. 100 mM phosphate buffer (pH 6.5 – 7.4) was added to lyophilized PEP protein and the suspension was placed on ice for 2 – 4 h to promote gelation. Fluorescent hydrogels were prepared by adding low concentrations of labeled PE$_C$P to normal PEP networks (typically, PE$_C$P:PEP mass ratios of 1:50 and 1:100 were used). Dye conjugation to cysteine-containing probes was performed as described previously (*18*).

Rheological analysis of gels. Oscillatory shear rheology was performed on 10% (*w*/*v*) PEP hydrogels using an ARES-RFS strain-controlled rheometer (TA Instruments) equipped with a cone-and-plate geometry. The outer edge of the plate was coated with mineral oil in order to minimize evaporation from the exposed gel. Strain sweeps identified a linear regime between 0.1 – 10% strain at 10 rad s^{-1}. Frequency sweeps were performed at a fixed strain amplitude of 1% between 0.01 and 100 rad s^{-1}. Temperature data was collected at 1% strain and 10 rad s^{-1}, at 5 °C intervals between 25 °C and 60 °C.

Cloud-point measurements. Protein solutions were prepared at concentrations ranging from 1 to 10% (*w*/*v*) in 100 mM phosphate buffer, pH 6.5 – 7.4. Solutions of PEP above 2 – 3% formed viscoelastic gels, whereas below 2% the solutions flowed easily. Solutions and gels were loaded between the two halves of a disassembled quartz cuvette. The cuvette was

assembled by pressing the two halves together, which sandwiched the gel within a 0.1 cm thick cavity. Roughly 400 μL of gel was required to fill the cuvette. The absorbance at 650 nm in response to temperature was monitored continuously on a Cary 100 Bio UV-Vis spectrometer equipped with temperature control. Gels were typically heated from 25 °C to 95 °C, held at 95 °C for 5 min, then cooled to 5 °C. The heating and cooling rates were held constant at 1 – 3 °C min^{-1}, with minimal differences observed between the faster and slower rates. Prior to cloud-point measurements on the "E_C" protein, a 5% solution was placed at 4 °C on a rotator plate for 3 – 4 days to promote oxidative crosslinking of the thiol groups.

3.6.2 Development of Phase Patterns

Imaging of spontaneous pattern formation and phase separation in labeled PEP hydrogels was performed on a Zeiss LSM 880 confocal microscope (488 nm with 10 – 20X objectives) equipped with a "Delta T" heated stage programmed to cycle between 25 °C and 50 °C within 60 seconds (Bioptechs, Butler PA). Labeled gels were placed on an ITO-coated, thermally conductive Delta T culture dish and sealed beneath a coverslip using 120 μm Secure-Seal spacers (Life Technologies). Image analysis was performed in MATLAB. FRAP experiments were performed on a Zeiss LSM 880 equipped with a 25 mW Argon laser. Recovery curves were fit to an effective diffusion model using the MATLAB function *nlinfit* (*18, 34*).

Patterning experiments were performed on a Zeiss LSM 5 Exciter equipped with a 25 mW Argon laser (458, 488 and 514 nm) and a 25 mW Diode (405 nm) laser. All laser lines, at maximum power, were typically activated during the photobleach. Bleach spot sizes ranged

from 100 – 2000 μm^2. Bleaching of a 500 μm^2 (a = 12.5 μm radius) circle at a scan rate of 4 μm s^{-1} required roughly 2000 scans to ensure efficient bleaching of fluorescein. Bleaching of larger spot sizes (2000 μm^2, a = 25 μm) was usually performed at a scan rate of 1 μm s^{-1}. Typical bleaching times varied from 2 – 10 min, depending on the size of the bleach spot and the total number of scans (2000 – 5000 scans). The total incident power emitted from the Argon laser during a typical fluorescein photobleach was measured to be ~1 mW using a power meter. At 1 mW incident power, the average irradiance (power density) was estimated to be 50 W cm^{-2}. After bleaching of the desired pattern, the sample was allowed to recover for 15 – 30 min. Gels were then slowly heated to 50 °C at rate of 2 – 3 °C min^{-1} using a standard heated stage and an aluminum coverslip mount.

Oxidative crosslinking studies. Gels were prepared at 5% in 100 mM phosphate buffer pH 7, supplemented with 25 μM free fluorescein or Rose Bengal, with or without 100 mM NaN_3. Gels were sealed between two coverslips, separated by a 0.030 in sheet of PDMS. Sample irradiation was performed using a Coherent Innova 70 CW Ar-Ion laser. The total incident beam power at 488 nm was fixed at 250 – 300 mW using a circular beam spot with a diameter of roughly 0.8 cm. The irradiance (power density) was estimated to be 0.5 W cm^{-2}. Gels were irradiated for 2 h, then solubilized in 8 M urea and crosslinking was assessed by SDS-PAGE under non-reducing conditions.

3.6.3 Supplementary Tables

Supplementary Table 3.1. Plasmids and amino acid sequences of phase programmable proteins. Protein coding sequences were confirmed by double-stranded DNA sequencing. Each "P" domain is highlighted in blue, and the "E" domain is highlighted in gray. Cysteine residues are highlighted in red.

Plasmid	Protein	Molecular Weight (Da)
pET15b-PEP	PEP	32,047
MKGSHHHHHHHVDGSGSGSGSGSGSGAPQMLRELQETNAALQDVRELLRQ QVKEITFLKNTVMESDASGSGSGSGSGSGSGLDGHGVGVPGVGVPGVGVPG EGVPGVGVPGVGVPGVGVPGVGVPGEGVPGVGVPGVGVPGVGVPGVGVPG EGVPGVGVPGVGELYAVTGRGDSPASSAPIATSVPGVGVPGVGVPGEGVPGV GVPGVGVPGVGVPGVGVPGEGVPGVGVPGVGVPGVGVPGVGVPGEGVPGV GVPGVGVPGGLLDGSGSGSGSGSGSGAPQMLRELQETNAALQDVRELLRQQ VKEITFLKNTVMESDASGSGSGSGSGSGLEMHHHHHHK*		
pET15b-PE$_C$P	PE$_C$P	32,151
MKGSHHHHHHHVDGSGSGSGSGSGSGAPQMLRELQETNAALQDVRELLRQ QVKEITFLKNTVMESDASGSGSGSGSGSGSGLDGHGVGVPGVGVPGVGVPG EGVPGVGVPGVGVPGVGVPGVGVPGEGVPGVGVPGVGVPGVGVPGVGVPG EGVPGVGVPGVGELCYAVTGRGDSPASSAPIATSVPGVGVPGVGVPGEGVPG VGVPGVGVPGVGVPGVGVPGEGVPGVGVPGVGVPGVGVPGVGVPGEGVPG VGVPGVGVPGGLLDGSGSGSGSGSGSGAPQMLRELQETNAALQDVRELLRQ QVKEITFLKNTVMESDASGSGSGSGSGSGLEMHHHHHHK*		
pQE80L-E	E	17,670
MKGSSHHHHHHVDGHGVGVPGVGVPGVGVPGEGVPGVGVPGVGVPGVGVP GVGVPGEGVPGVGVPGVGVPGVGVPGVGVPGVGVPGEGVPGVGVPGVGELYAVTG RGDSPASSAPIATSVPGVGVPGVGVPGEGVPGVGVPGVGVPGVGVPGVGVP GEGVPGVGVPGVGVPGVGVPGVGVPGVGVPGEGVPGVGVPGVGVPGVGVPGGLLEWKKM*		
pQE80L-E$_C$	E$_C$	17,706
MKGSSHHHHHHVDGHGVGVPGVGVPGVGVPGEGVPGVGVPGVGVPGVGVP GVGVPGEGVPGVGVPGVGVPGVGVPGVGVPGVGVPGEGVPGVGVPGVGELYAVTG RGDSPACSAPIATSVPGVGVPGVGVPGEGVPGVGVPGVGVPGVGVPGVGVP GEGVPGVGVPGVGVPGVGVPGVGVPGVGVPGEGVPGVGVPGVGVPGVGVPGGLLEWKKM*		

3.6.4 Supplementary Figures

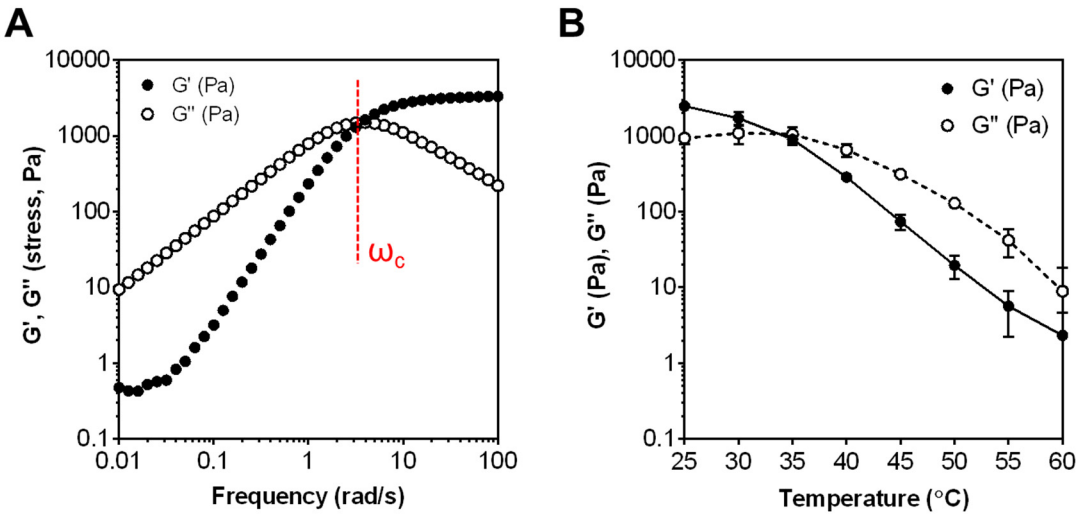

Supplementary Figure 3.1. Temperature-dependent rheology of PEP hydrogels. (**A**) Frequency sweep of 10% (*w*/*v*) gels prepared in 100 mM phosphate buffer at a fixed strain amplitude of 1% (25 °C). The network behaves as a viscous liquid at low frequencies ($G' < G''$) but transitions to elastic-dominated behavior at high frequencies ($G' > G''$). This transition occurs at a critical frequency ω_c, corresponding to the dominant stress relaxation mode of the physical network. (**B**) Storage (G') and loss (G'') moduli were measured for a 10% gel at 1% strain, 10 rad s^{-1} at various temperatures (n = 2, mean ± SD). Although the viscous loss modulus dominates at high temperatures, weak crosslinking is still evident.

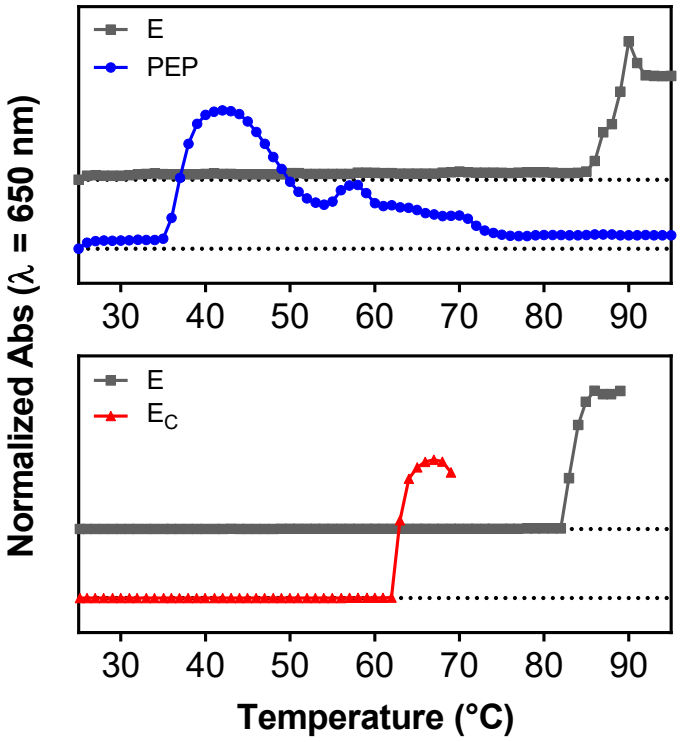

Supplementary Figure 3.2. Crosslinking affects the LCST of elastin-like proteins. Proteins were dissolved at a concentration of 5% in 100 mM phosphate buffer (pH 6.5 – 7.4) and heated to 95 °C at a rate 1 °C min^{-1}. The onset of turbidity was monitored at 650 nm. (*Top*) The predicted LCST of E based on its repeat sequence (70 °C) is close to its observed transition temperature (80 - 90 °C), whereas the transition temperature of gelled PEP is much lower (38 °C). (*Bottom*) The presence of an oxidized thiol (dimerization) in E_C depresses its LCST by ~20 °C relative to E.

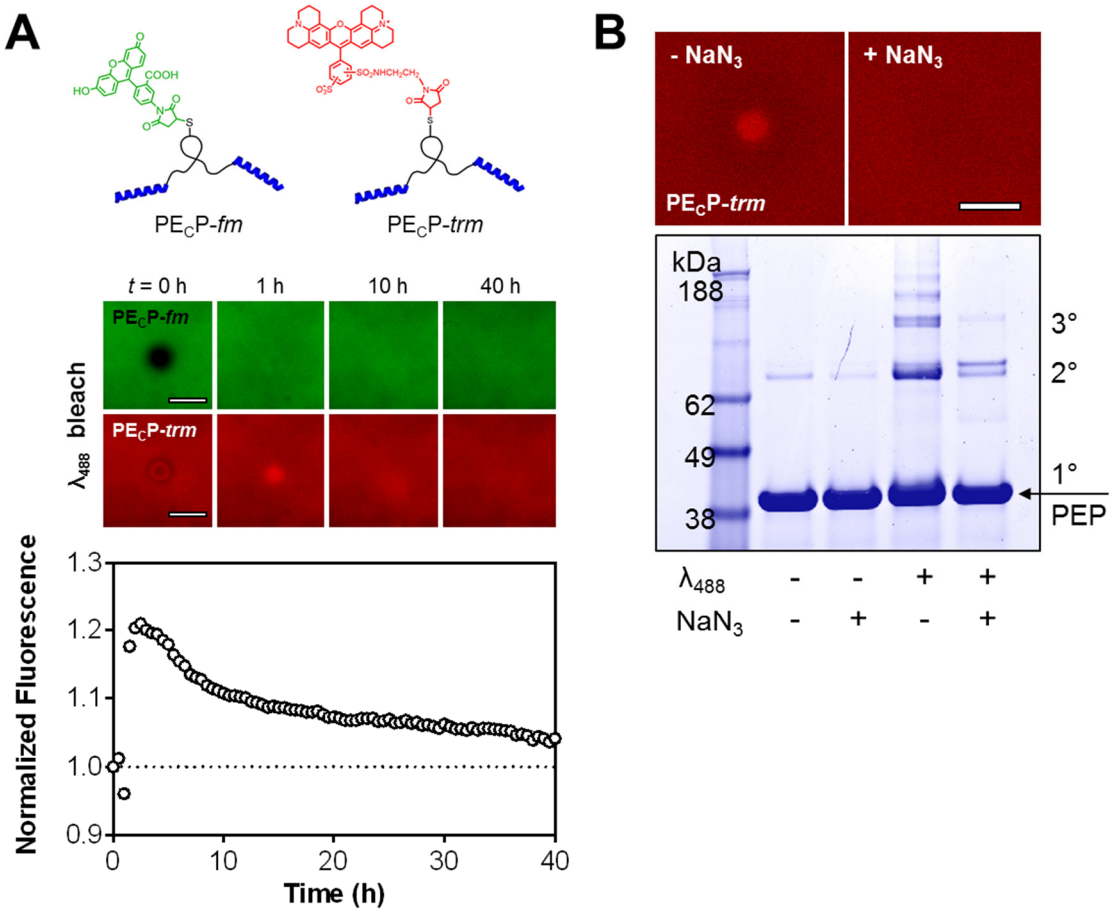

Supplementary Figure 3.3. Photobleaching promotes covalent interchain crosslinking and subsequent probe enrichment in bleach spots. (A) 5% gels were labeled with green (PE_CP-*fm,* 490Ex/525Em) and red (PE_CP-*trm*, 596Ex/615Em) probes and photobleached (spot radius $a = 25$ µm, λ_{488} bleach). Fluorescence recovery was monitored at 25 °C. Red probes diffused into photobleached volumes and remained enriched for several hours. Scale bar = 100 µm. (B) (*Top*) Photobleaching promotes covalent interchain crosslinking by singlet oxygen generation. The presence of 100 mM NaN_3, a strong singlet oxygen quencher, prevented probe enrichment in 5% gels labeled with red and green probes (λ_{488} bleach). (*Bottom*) Bulk irradiation of 5% gels (488 nm, 500 mW cm^{-2}) containing 25 µM free fluorescein promoted covalent multimer formation of PEP chains. Multimerization was suppressed by the presence of 100 mM NaN_3. Similar results were obtained with Rose Bengal, a highly efficient singlet oxygen generator, in place of fluorescein. All scale bars = 100 µM.

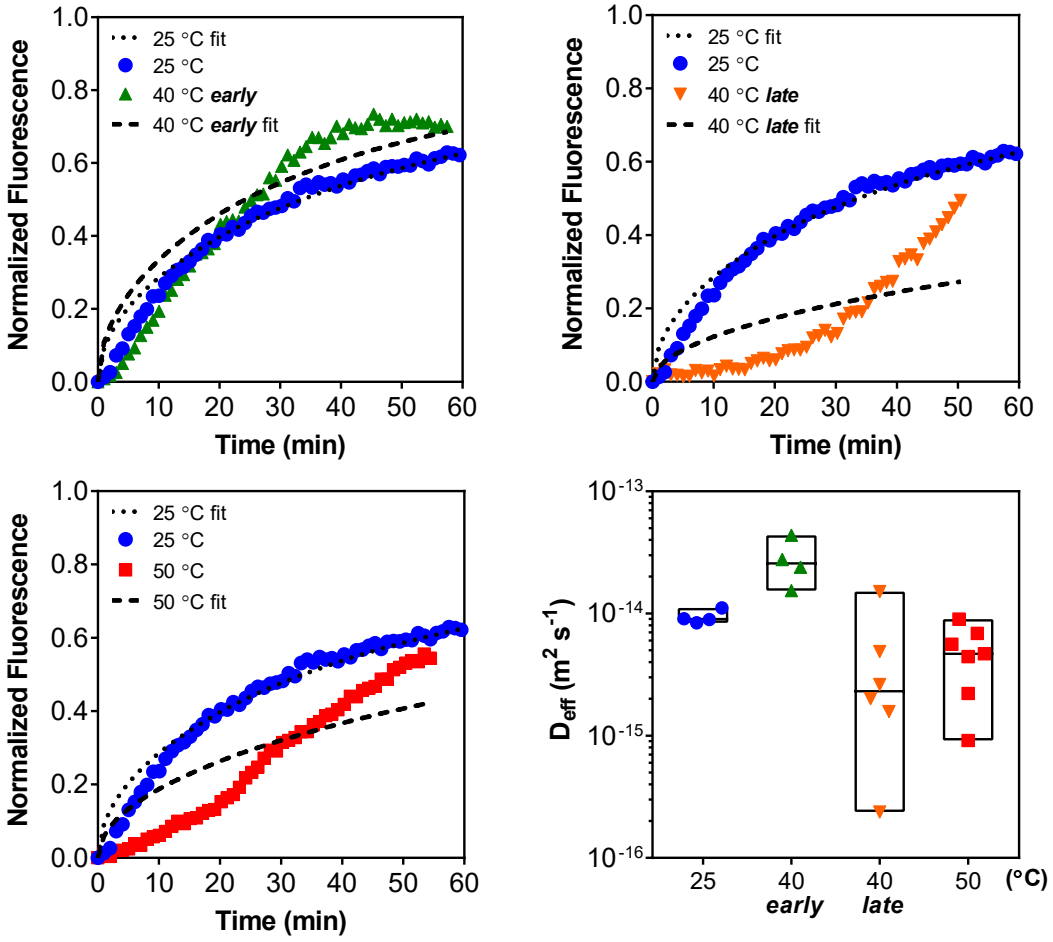

Supplementary Figure 3.4. Anomalous FRAP behavior above the LCST is poorly fit by standard FRAP models. Shown are representative FRAP traces acquired in a 10% PEP gel at 40 °C and 50 °C, along with their corresponding fits assuming Fickian diffusion (dashed black lines). Poor fits and the highly heterogenous nature of phase separated samples made reliable determination of the effective diffusion coefficient (D_{eff}) difficult.

3.7 References and Notes

1. F. S. Bates, Polymer-Polymer Phase-Behavior. *Science* **251**, 898-905 (1991).

2. B. de Boer *et al.*, Supramolecular self-assembly and opto-electronic properties of semiconducting block copolymers. *Polymer* **42**, 9097-9109 (2001).

3. K. Sivula, Z. T. Ball, N. Watanabe, J. M. J. Fréchet, Amphiphilic Diblock Copolymer Compatibilizers and Their Effect on the Morphology and Performance of Polythiophene:Fullerene Solar Cells. *Adv. Mater.* **18**, 206-210 (2006).

4. G. B. Wei, P. X. Ma, Structure and properties of nano-hydroxyapatite/polymer composite scaffolds for bone tissue engineering. *Biomaterials* **25**, 4749-4757 (2004).

5. H. Tanaka, Formation of Network and Cellular Structures by Viscoelastic Phase Separation. *Adv. Mater.* **21**, 1872-1880 (2009).

6. H. Tanaka, Unusual Phase-Separation in a Polymer-Solution Caused by Asymmetric Molecular-Dynamics. *Phys Rev Lett* **71**, 3158-3161 (1993).

7. T. Taniguchi, A. Onuki, Network Domain Structure in Viscoelastic Phase Separation. *Phys Rev Lett* **77**, 4910-4913 (1996).

8. W. W. Mullins, The Statistical Self-Similarity Hypothesis in Grain-Growth and Particle Coarsening. *J Appl Phys* **59**, 1341-1349 (1986).

9. H. Tanaka, Universality of viscoelastic phase separation in dynamically asymmetric fluid mixtures. *Phys Rev Lett* **76**, 787-790 (1996).

10. A. J. Wagner, J. M. Yeomans, Breakdown of Scale Invariance in the Coarsening of Phase-Separating Binary Fluids. *Phys Rev Lett* **80**, 1429-1432 (1998).

11. S. Tanaka, M. Ataka, K. Ito, Pattern formation and coarsening during metastable phase separation in lysozyme solutions. *Phys Rev E* **65**, (2002).

12. H. Tanaka, Y. Nishikawa, Viscoelastic Phase Separation of Protein Solutions. *Phys Rev Lett* **95**, 078103 (2005).

13. T. Hajime, N. Yuya, K. Takehito, Network-forming phase separation of colloidal suspensions. *Journal of Physics: Condensed Matter* **17**, L143 (2005).

14. S. Tanaka *et al.*, Kinetics of phase separation and coarsening in dilute surfactant pentaethylene glycol monododecyl ether solutions. *J Chem Phys* **135**, (2011).

15. V. N. Malashkevich, R. A. Kammerer, V. P. Efimov, T. Schulthess, J. Engel, The crystal structure of a five-stranded coiled coil in COMP: A prototype ion channel? *Science* **274**, 761-765 (1996).

16. L. J. Dooling, M. E. Buck, W. B. Zhang, D. A. Tirrell, Programming Molecular Association and Viscoelastic Behavior in Protein Networks. *Adv Mater* **28**, 4651-4657 (2016).

17. B. D. Olsen, J. A. Kornfield, D. A. Tirrell, Yielding Behavior in Injectable Hydrogels from Telechelic Proteins. *Macromolecules* **43**, 9094-9099 (2010).

18. P. B. Rapp *et al.*, Analysis and Control of Chain Mobility in Protein Hydrogels. *J. Am. Chem. Soc.* **139**, 3796-3804 (2017).

19. D. E. Meyer, A. Chilkoti, Quantification of the effects of chain length and concentration on the thermal behavior of elastin-like polypeptides. *Biomacromolecules* **5**, 846-851 (2004).

20. R. A. McMillan, V. P. Conticello, Synthesis and characterization of elastin-mimetic protein gels derived from a well-defined polypeptide precursor. *Macromolecules* **33**, 4809-4821 (2000).

21. D. W. Urry, Physical Chemistry of Biological Free Energy Transduction As Demonstrated by Elastic Protein-Based Polymers. *The Journal of Physical Chemistry B* **101**, 11007-11028 (1997).

22. Subtle changes to the refolding procedure employed during protein purification could significantly shift this first transition temperature (see Materials and Methods). We take this as further evidence that the LCST depends on the crosslinked state.

23. T. Luo, K. L. Kiick, Noncovalent Modulation of the Inverse Temperature Transition and Self-Assembly of Elastin-b-Collagen-like Peptide Bioconjugates. *J. Am. Chem. Soc.* **137**, 15362-15365 (2015).

24. F. G. Quiroz, A. Chilkoti, Sequence heuristics to encode phase behaviour in intrinsically disordered protein polymers. *Nat Mater* **14**, 1164-1171 (2015).

25. J. S. Haghpanah *et al.*, Artificial Protein Block Copolymers Blocks Comprising Two Distinct Self-Assembling Domains. *ChemBioChem* **10**, 2733-2735 (2009).

26. C. B. Qian, S. J. Mumby, B. E. Eichinger, Phase-Diagrams of Binary Polymer-Solutions and Blends. *Macromolecules* **24**, 1655-1661 (1991).

27. E. L. Cheluget, M. E. Weber, J. H. Vera, Modifications of the Flory-Huggins-Goldstein Model for Accurate Description of Closed-Loop Phase-Diagrams. *Chem Eng Sci* **48**, 1415-1426 (1993).

28. S. K. Gunasekar *et al.*, N-Terminal Aliphatic Residues Dictate the Structure, Stability, Assembly, and Small Molecule Binding of the Coiled-Coil Region of Cartilage Oligomeric Matrix Protein. *Biochemistry* **48**, 8559-8567 (2009).

29. H. Tanaka, T. Araki, T. Koyama, Y. Nishikawa, Universality of viscoelastic phase separation in soft matter. *J Phys-Condens Mat* **17**, S3195-S3204 (2005).

30. H. Tanaka, Viscoelastic phase separation. *J Phys-Condens Mat* **12**, R207-R264 (2000).

31. S.-W. Song, J. M. Torkelson, Coarsening Effects on Microstructure Formation in Isopycnic Polymer Solutions and Membranes Produced via Thermally Induced Phase Separation. *Macromolecules* **27**, 6389-6397 (1994).

32. Y. A. Li *et al.*, Mobility of lysozyme inside oxidized starch polymer microgels. *Soft Matter* **7**, 1926-1935 (2011).

33. P. Gribbon, T. E. Hardingham, Macromolecular diffusion of biological polymers measured by confocal fluorescence recovery after photobleaching. *Biophys J* **75**, 1032-1039 (1998).

34. B. L. Sprague, R. L. Pego, D. A. Stavreva, J. G. McNally, Analysis of binding reactions by fluorescence recovery after photobleaching. *Biophys J* **86**, 3473-3495 (2004).

35. A. K. Gaigalas, L. Wang, K. D. Cole, E. Humphries, Photodegradation of fluorescein in solutions containing n-propyl gallate. *J Phys Chem A* **108**, 4378-4384 (2004).

36. F. Stracke, M. Heupel, E. Thiel, Singlet molecular oxygen photosensitized by Rhodamine dyes: correlation with photophysical properties of the sensitizers. *J Photochem Photobiol A* **126**, 51-58 (1999).

37. H. R. Shen, J. D. Spikes, P. Kopeckova, J. Kopecek, Photodynamic crosslinking of proteins .2. Photocrosslinking of a model protein-ribonuclease A. *J Photochem Photobiol B* **35**, 213-219 (1996).

38. M. P. Sheetz, D. E. Koppel, Membrane Damage Caused by Irradiation of Fluorescent Concanavalin-A. *Proc Natl Acad Sci USA* **76**, 3314-3317 (1979).

39. M. J. Davies, Singlet oxygen-mediated damage to proteins and its consequences. *Biochem Bioph Res Co* **305**, 761-770 (2003).

40. L. J. Dooling, D. A. Tirrell, Engineering the Dynamic Properties of Protein Networks through Sequence Variation. *ACS Central Science* **2**, 812-819 (2016).